Renewable Energy 177 (2021) 976–991

Contents lists available at ScienceDirect

Renewable Energy

journal homepage: www.elsevier.com/locate/renene

Closed-loop geothermal energy recovery from deep high enthalpy systems

Wanju Yuan *, Zhuoheng Chen , Stephen E. Grasby , Edward Little

Geological Survey of Canada, 3303 33rd Street, NW, Calgary, T2L 2A7, Alberta, Canada

A R T I C L E I N F O

Article history:
Received 28 October 2020
Received in revised form
4 May 2021
Accepted 4 June 2021
Available online 7 June 2021

Keywords:
Closed-loop geothermal technology
Thermodynamics
Technology evaluation
Analytical modeling
Sensitive analysis

A B S T R A C T

Closed-loop geothermal energy recovery technology has advantages of being independent of reservoir fluid and permeability, experiencing less parasitic load from pumps, and being technologically ready and widely used for heat exchange in shallow geothermal systems. Commercial application of closed-loop geothermal technology to deep high-enthalpy systems is now feasible given advances in drilling technology. However, the technology it uses has been questioned due to differences in heat transport capacities of convective flow within the wellbores and conductive flux in the surrounding rock. Here we demonstrate that closed-loop geothermal systems can provide reasonable temperature and heat duty for over 30 years using multiple laterals when installed in a suitable geological setting. Through use of two analytical methods, our results indicate that the closed-loop geothermal system is sensitive to reservoir thermal conductivity that controls the level of outlet temperature and interference between wells over time. The residence time of the fluid in the horizontal section, calculated as a ratio of the lateral length to flow rate, dictates heat transport efficiency. A long vertical production section could cause large drops in fluid temperature in a single lateral production system, but such heat loss can be reduced significantly in a closed-loop system with multiple laterals.

1. Introduction

Geothermal energy is one of a suite of renewable energies that can help to reduce global CO_2 emissions [1] and transition modern-day society to a lower-carbon economy [2]. While having the benefit of being able to provide baseload power supply, geothermal development comes with the challenge of finding thermal reservoirs that have porosity and permeability suitable for economic production [3]. Such traditional geothermal development typically involves drilling a production well, for extraction of deep thermal waters, along with a re-injection well to dispose of produced fluids after heat extraction. In the subsurface, heat is carried by fluids transported through porous and/or fractured media towards the production well [4], and both heat conduction and convection affect the overall heat production efficiency (Fig. 1). In contrast, shallow geothermal-exchange systems that have been widely used around the world for space heating [5] make use of a closed-loop system that circulates a working fluid to extract and store heat underground (depending on the season). Advances in drilling technology have led to consideration of such closed-loop systems for development of deeper (higher temperature) geothermal resources (e.g., Eavor Technologies, 2021; [6]. Such closed-loop systems are similar to geothermal-exchange, but at a much larger scale to utilize deeper high-enthalpy resources [5]. In concept, closed-loop technology applies thousands of meters long horizontal wellbores in the target thermal reservoir that are connected by two vertical wells, one inlet well, and one production well (Fig. 2). A low temperature working fluid is injected from the inlet, heated mostly through the horizontal interval in a geothermal reservoir with proper thermal properties, and the heat energy is harvested at the outlet for heating and power generation purposes. In contrast to a traditional geothermal energy system, a closed-loop system uses a working fluid that circulates with a designed flow rate. In this sense the system is independent of permeability, greatly reducing the exploration risk, and there are no associated environmental or scaling issues with production of geothermal fluids to surface (Fig. 2). A key limitation though is that heat in a closed-loop system can only be transported from the reservoir to the wellbore by heat conduction [7], while within the wellbore, convection dominates.

Geothermal energy resources are widely distributed in Canada,

* Corresponding author.
E-mail address: wanju.yuan@canada.ca (W. Yuan).

https://doi.org/10.1016/j.renene.2021.06.028
0960-1481/

Nomenclature

A	cross section area of lateral wellbore, m^2
a	factors in Matrix need to multiply heat flux terms
C	right hand side value of the matrix calculation
c	specific heat capacity, J/kg/K
D	Inner diameter of lateral wellbore, m
erf	error function
exp	exponential function
h	depth of the reservoir in case study of heat exchange in vertical wellbore, m
ln	the natural logarithm
L	length of the lateral wellbore, m
N	number of segments of lateral wellbore for analytical modeling
N_L	numerical calculation number in Stehfest inverse algorism
N_l	number of laterals
q	instantaneous conductive heat inflow, W
q_c	conductive heat flux from reservoir to wellbore under unit length, W/m
q_{cu}	conductive heat flux under unit length and temperature difference, W/m/K
q_f	flow rate per lateral, m^3/hr
Q_o	cumulative heat amount produced out by working fluids, J
Q_r	cumulative heat loss from the reservoir, J
r_i	the radius of investigation in geothermal industry, m
s	Laplace transform parameter
t	time, s
T	temperature, K
ΔT	temperature change caused by source/sink, K
V_i	functions in Stehfest inverse algorism
v	velocity of the working fluid in lateral wellbore, m/s
x	x coordinate location, m
y	y coordinate location, m
z	z coordinate location, m

Greek symbols

α	thermal diffusivity of reservoir, m^2/s
λ	thermal conductivity of reservoir, W/m/K
ρ	density, kg/m^3
τ	instantaneous source time, s

Subscripts

ave	average value
e	boundary coordinates of the reservoir
f	fluid
inlet	the variable at the inlet
l	property of lateral wellbore part
L	one endpoint of this segment
mid-point	mid-point of each segment
outlet	the variable at the outlet
r	reservoir
R	one endpoint of this segment
s	surface
seg	property of the segment
sx	source/sink function in x direction
sy	source/sink function in y direction
sz	source/sink function in z direction
v	property of vertical wellbore part
#1	functions from sub-system #1
#2	functions from sub-system #2
11,…1N,…N1,…NN	location of factors in matrix a
1,2,…,N	location of values in matrix c

Superscripts

i	the variable, or function of the ith segment
1,2,…,N	the variable of the corresponding segment
*	residence time of working fluids in horizontal wellbore
‘	heat source/sink location

Acronyms

NW	northwest
PTA	Pressure Transient Analysis
RTA	Rate Transient Analysis
WCSB	Western Canadian Sedimentary Basin

with the highest potential areas occurring in the western and northwestern parts of the country [8–14]. Recently many geothermal energy projects have been initiated in Canada (e.g. [15–17], to demonstrate either the resource development technology or geothermal resource concepts. Notable, in 2019, Eavor drilled the Eavor-Lite™ closed-loop project in Alberta, Canada as a full-scale prototype of the drilling technology required (but not at full development depth), and to validate the thermosiphon effects [16].

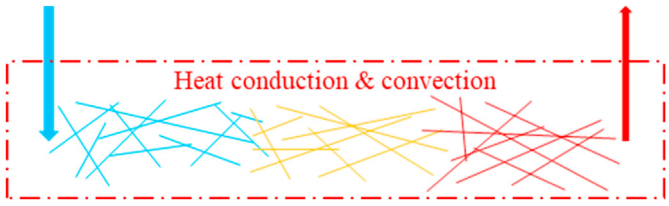

Fig. 1. Schematic diagram of the heat transfer mechanism in conventional geothermal energy recovery with a pair of vertical wells. Colours represent working fluid temperatures ranging from cold (blue) to hot (red).

Recent research work on closed-loop geothermal heat production focuses on shallow geothermal systems with four major styles of heat exchangers (single U-tube, double U-tube, coaxial centred, and coaxial annular) [18]. Evaluation on long-lateral U shape closed-loop system usually needs to apply numerical simulations on the discretized reservoir with local fine grided meshing near wellbore [19,39]. Few works used analytical modeling of long-lateral U shape closed-loop system in deep high temperature reservoir. To evaluate the thermodynamic efficiency of a closed-loop multilateral wellbore system, at reservoir temperatures and depths, we developed two analytical methods to model energy production. These two analytical methods, coupled with a transient heat transfer process, simplify nonisothermal flow in a closed-loop system. The meshed-free modeling provides an accurate heat production output with less computation time. Key parameters of the system and its sensitivity have been examined to help better understand key controls on this geothermal energy recovery technology. The overall thermal production and heat duty are also discussed.

We note that a deep closed-loop system would require advanced horizontal drilling techniques and bear additional costs. Drilling

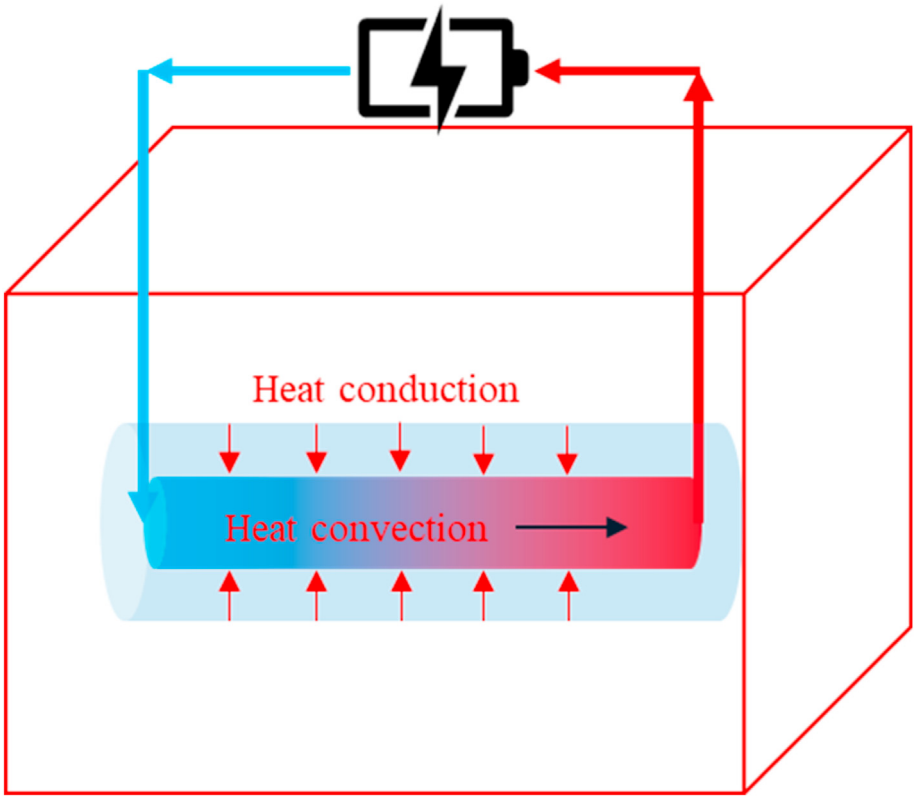

Fig. 2. Schematic diagram of a closed-loop geothermal energy recovery system and its heat transfer mechanism. Colours represent working fluid temperatures ranging from cold (blue) to hot (red). The battery symbol reflects end heat usage (direct heat use and/or power generation).

techniques evolve quickly as evidenced by oil and gas drilling for shale gas production as well as drilling in the enhanced geothermal system [20] to overcome various difficulties, such as long-lateral directional drilling, multilateral completions, high-temperature effects, thermal expansion of casing strings, hardness [21], and large diameters [22]. Several recent geothermal projects in Canada and elsewhere have successfully completed, or planned their wells in large depth (>3000 m) [15,23,24]. And the recently completed long lateral demonstration closed-loop system drilled in Alberta by Eavor [16] demonstrates the state of the art of long-lateral directional drilling in geothermal production. Other new advancement includes the sealed lateral wellbore with the absence of casing to enhance the heat transfer efficiency [25]. However, the technical difficulties of drilling and costs are not the intension of this study. This study is focused on analytical methods that would adequately characterize the closed-loop system and allow evaluation of the critical factors that affect the heat transmission in such systems.

However, there is no publicly information available to validate the model and evaluate the heat exchange capacity in such a system. This study examines the major factors affecting the thermal transporting capacity for the closed-loop system and its applicability to the sedimentary basin. In Alberta, the huge amount of data from oil and gas exploration and production wells allows for estimation and mapping of the thermal-physical properties of the sedimentary layers. The oil and gas industry is looking for practical technologies for making a transition from fossil fuel to renewable energy. If applicable in some suitable geological settings, this closed-loop system would be used to help the oil and gas industry to reduce CO_2 emission by geothermal-assisted fossil fuel production, or converting oil and gas well to a geothermal well when depleted.

2. Physical and mathematical model

Assumptions. The closed-loop geothermal recovery technology applies a sealed horizontal wellbore along the target thermal reservoir (Fig. 2). The working fluid (e.g., water, or other fluids with thermosiphon effects) circulates within the sealed wellbore from the vertical inlet through the horizontal leg, to the production well. The working fluid is heated by the thermal reservoir as it flows to the outlet that connects to a power generator or a heat user. The major assumptions to model this system are as follows:

1) Heat energy resource comes from geothermal heat flux from Earth and is stored in a geothermal reservoir that has specific thermal-physical properties allowing extraction of the energy resource through heat exchange by water circulation in tubing efficiently.
2) The dimension of the geothermal reservoir is far greater than the extent of a horizontal wellbore in the closed-loop system so that reservoir boundary will not affect the production performance.
3) The initial heat reservoir is assumed to be in thermal equilibrium. In this model, the horizontal well acts as the only sink to extract heat energy out of the system. The heat source from Earth will not affect the heat extraction performance due to low thermal diffusivity and large reservoir dimension.
4) Pure heat conduction in the thermal reservoir. No natural or induced heat convection by fluid flow in the surrounding rock mass occurs. A heat convection mechanism dominates the heat transfer process along the fluid flow direction within the horizontal wellbore system. The heat transfer within cross-section of the working fluid is neglected based on following assumption.

5) The diameter of the horizontal wellbore is extremely small compared with the dimension of the thermal reservoir. The heat transfer within the wellbore is simplified as a 1D heat convection process, and the thermal resistance by convective flow is neglected in this study. The temperature profile within each cross-section of the wellbore is assumed uniform but transient.
6) The overall thermal resistance between fluid and rock is neglected including the potential resistance from the steel tube wall, casing, and cement ring. In the closed-loop system, it is critical to enlarge the contact area between the reservoir and working fluids, and reduce the thermal resistance to improve the thermodynamic performance. Innovations of the sealed horizontal portion without casing have also been commercialized in long lateral closed-loop geothermal energy production [16,25]. As a result, this study will focus on the general geothermal production evaluation without consideration of the overall thermal resistance within the wellbore.
7) The working fluid flow rate is constant throughout the thermal production period.
8) Thermal properties of the working fluid and the reservoir, such as thermal conductivity and volumetric heat capacity are constant.

Continuity equation. A small volume of the horizontal wellbore and its near wellbore region has been chosen (Fig. 3) to demonstrate the heat balance mathematically using the following equation:

$$A\rho_f c_f \frac{\partial T(x,t)}{\partial t} = -vA\rho_f c_f \frac{\partial T(x,t)}{\partial x} + q_c(x,t) \tag{1}$$

The heat balance for each location in the horizontal wellbore is based on the law of energy conservation. The left-hand side of Eq. (1) is the heat amount accumulated at a certain location x at time t. The first term in the right-hand side is the amount of heat transferred by convection in the horizontal well. Because of the high velocity of the convective flow, heat brought by thermal conduction is negligible. This contrasts with conventional geothermal energy systems, where the working fluid is flowing at low velocity through porous media, and both heat conduction and convection contribute significantly to the overall heat transfer performance (Fig. 1). The second term of the right-hand side of the equation is the heat transferred by conduction from rock forming the thermal reservoir surrounding the wellbore. This transient heat flux, $q_c(x,t)$, is controlled by both the temperature difference between the outside and inside of the wellbore, and the thermal conductivity of the rock. We discuss the transient heat flux derivation later.

Initial and boundary conditions. The initial temperature of the reservoir, along with the fluid in the wellbore, is the reservoir temperature, T_r, K.

$$T(n, t=0) = T_r,\ n = x,\ y,\ z \tag{2}$$

The reservoir has a closed thermal boundary in each x, y, z direction. There is no heat communication at the outer boundary.

$$\frac{\partial T}{\partial n} = 0,\ n = x,\ y,\ z \tag{3}$$

3. Methodology

As mentioned before, determination of the conductive heal flux, $q_c(x,t)$ requires defining the temperatures of the surrounding rock (outside) and working fluid (inside) of the wellbore, which are unknown. The multilateral wellbore configuration adds additional complexity on transient heat flux calculation. In our study, two analytical methods were applied to tackle this dynamic heat transfer phenomenon. In general, the continuity equation needs to be Laplace transformed as:

$$s\overline{T} = -v\frac{\partial \overline{T}}{\partial x} + \frac{\overline{q_c}}{A\rho_f c_f} \tag{4}$$

where, s is the Laplace transform parameter; symbols with "-" means parameters in Laplace domain.

Duhamel's convolution theory method. The Duhamel's convolution theory has been widely used in Pressure Transient Analysis (PTA) and Rate Transient Analysis (RTA) in the oil and gas industry. Convolution theory has also been used by many researchers analyzing heat loss during steam injection for heavy oil recovery (e.g., [26,27]. In the convolution theory, the conductive heat flux, q_c, can be calculated as a convolution of temperature derivative with standard conductive heat flux under unit temperature difference:

$$q_c = \int_0^t \frac{\partial T(\tau)}{\partial \tau} \cdot q_{cu}(t-\tau)d\tau \tag{5}$$

In Eq. (5), q_{cu} is the conductive heat flux under unit temperature difference calculated from the standard source and sink functions [28]:

$$\Delta T = 1 = \int_0^t \frac{q_{cu}(\tau)}{2\pi\lambda} \frac{1}{\alpha(t-\tau)} exp\left[-\frac{(x-x')^2 + (y-y')^2}{4\alpha(t-\tau)}\right] d\tau \tag{6}$$

and in Laplace domain, q_{cu} can be calculated based on convolution theory:

$$\overline{q_{cu}} = \frac{s}{L[\xi(t)]} \tag{7}$$

$$\xi(t) = \frac{1}{2\pi\lambda\alpha t} exp\left[-\frac{(x-x')^2 + (y-y')^2}{4\alpha t}\right] \tag{8}$$

"L[]" means the value of original variables after Laplace transformation. In this work, Chebyshev's Theorem [29] was applied to calculate the numerical Laplace transformation value. And α is the thermal diffusivity of reservoir which can be defined as followed:

$$\alpha = \frac{\lambda}{\rho_r c_r} \tag{9}$$

When Laplace transformation applied to Eq. (5), the conductive heat flux from reservoir to horizontal wellbore can be derived as a function of the local temperature and the conductive heat flux under unit temperature difference:

$$\overline{q_c} = s \cdot \overline{T} \cdot \overline{q_{cu}} \tag{10}$$

Substituting Eq. (10) into Eq. (4), the outlet temperature in Laplace domain can be expressed as:

$$\overline{T_{outlet}} = \frac{(T_r - T_{inlet})}{s} \cdot exp\left(-\frac{sL}{Av\rho_f c_f} \cdot \overline{q_{cu}} - s \cdot \frac{L}{v}\right) \tag{11}$$

Natural Coupling Method. In more complicated situations, involving multilateral wells in a heterogeneous reservoir, a reservoir-scale analytical thermodynamic model is needed to evaluate the thermal production performance. In this study,

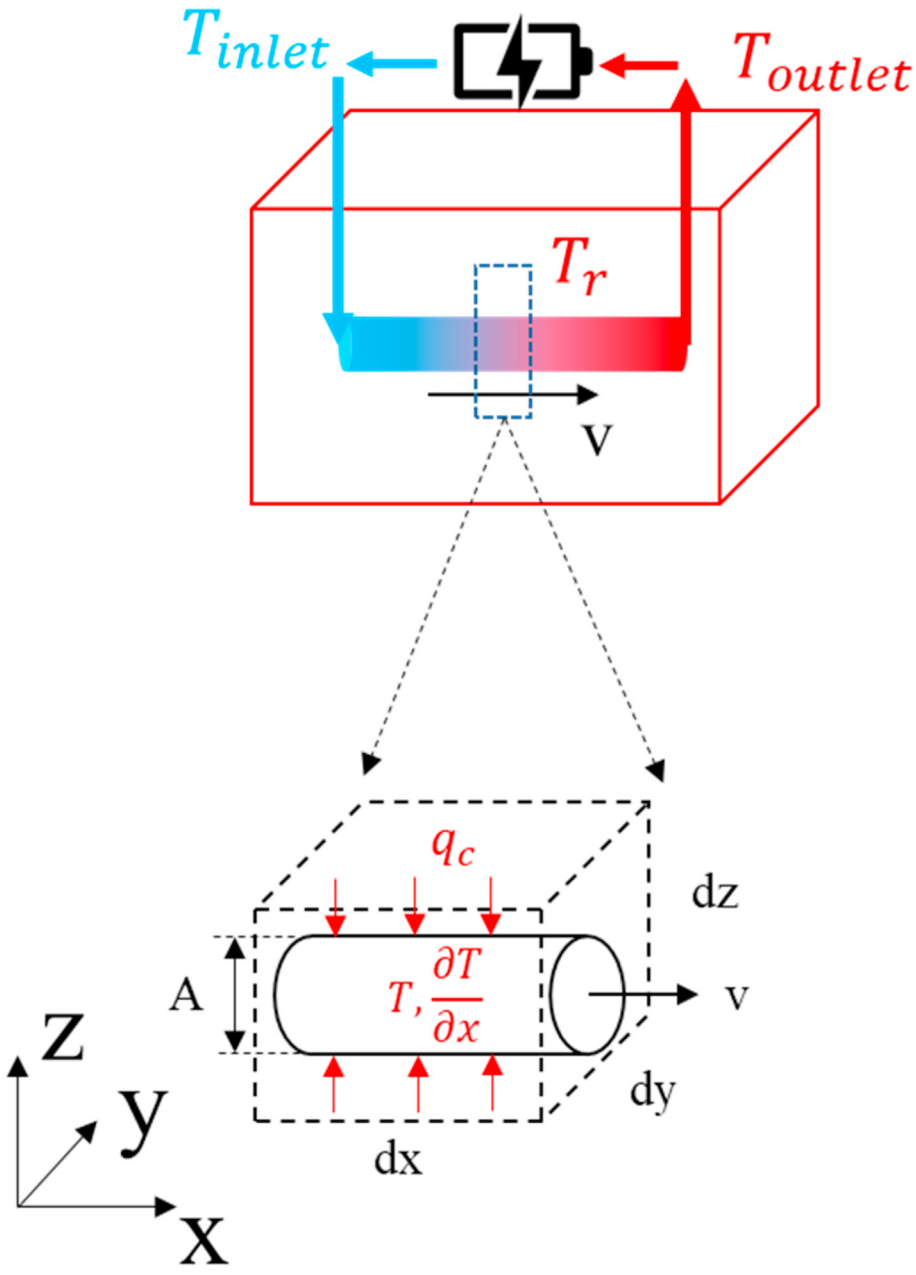

Fig. 3. Schematic diagram of fundamental heat transfer model of Closed-Loop geothermal energy recovery system.

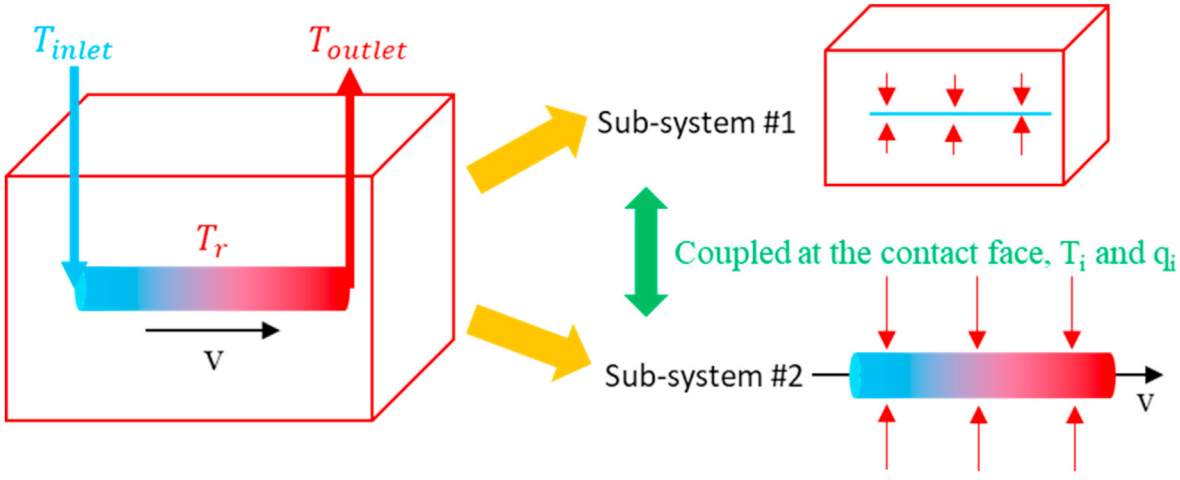

Fig. 4. Schematic diagram of two sub-systems examined in the Natural Coupling Method.

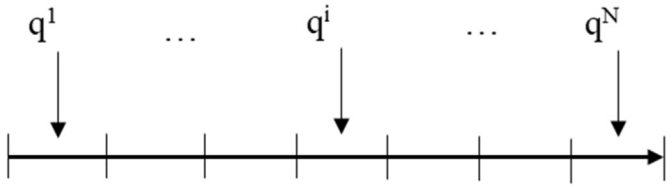

Fig. 5. Schematic diagram of N segments divided from the total length of lateral used in sub-system #1.

analytical reservoir modeling methodology has been applied to our problem using integration of instantaneous source and sink functions [28]. This methodology has been successfully applied to solving transient fluid flow problems in the oil and gas industry [30–34,40]. The original system can be seen as a combination of two separate sub-systems (Fig. 4). Sub-system #1 is a cubic shaped hot reservoir with a certain length line sink lying in the center of the reservoir. Heat is transferred into the line sink. Inflow heat flux varies in different part of the sink. Sub-system #2 is a cylinder-shaped system. The working fluid is transported in one direction at constant velocity. Along the direction of fluid movement, convective heat transfer dominates the overall performance, while conductive heat flux flows laterally.

In sub-system #1, the line source can be divided into N segments (Fig. 5). In each segment, the heat flux is uniform and the corresponding temperature change caused by this sink segment can be expressed as:

$$\Delta T^i = \int_0^t \frac{q^i(\tau)}{\rho_r c_r} \cdot T^i_{sx}(t-\tau) T^i_{sy}(t-\tau) T^i_{sz}(t-\tau) d\tau \tag{12}$$

$T^i_{sx}(t-\tau)$, $T^i_{sy}(t-\tau)$, $T^i_{sz}(t-\tau)$ are source/sink function in x, y, z direction, which can be expressed as following:

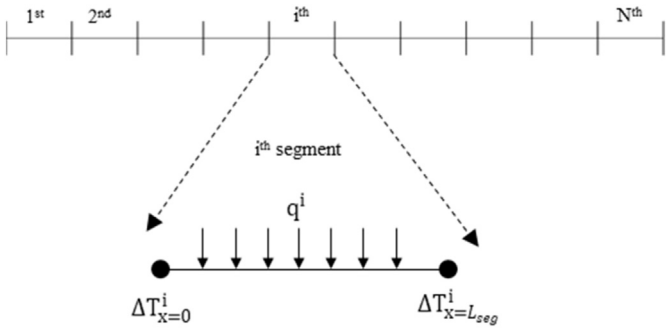

Fig. 6. Schematic diagram of sub-system #2 and its N segments.

As a result of the superposition principle, the temperature change at any evaluation point is the summation of the contributions from all horizontal source/sink segments:

$$\Delta T(x,y,z,t) = \sum_{i=1}^{N} \int_0^t \frac{q^i(\tau)}{\rho_r c_r} \cdot T^i_{sx}(t-\tau) T^i_{sy}(t-\tau) T^i_{sz}(t-\tau) d\tau \tag{18}$$

In sub-system #2, the wellbore is also divided into N segments (Fig. 6), and a uniform conducive heat flux is assumed along each horizontal interval. Each segment has the same temperature value at all joint points. As a result, the heat transfer governing equations in each segment can be expressed as:

$$\begin{cases} \dfrac{\partial \Delta T^i}{\partial t} = -v\dfrac{\partial \Delta T^i}{\partial x} + \dfrac{q^i}{AL_{seg}\rho_f c_f}, \ 0 \le x \le L_{seg} \\ \Delta T^i(x, t=0) = 0, \ 0 \le x \le L_{seg} \\ \Delta T^i(x=0, t) = \Delta T^{i-1}(x = L_{seg}, t) \\ \Delta T^i(x = L_{seg}, t) = \Delta T^{i+1}(x = 0, t) \end{cases} \tag{19}$$

$$T^i_{sx}(t-\tau) = \frac{1}{L_{seg}} \sum_{-\infty}^{\infty} \left\{ \frac{1}{2} erf\left[\frac{T^i_R - x + 2nx_e}{2\sqrt{\alpha(t-\tau)}}\right] - \frac{1}{2} erf\left[\frac{T^i_L - x + 2nx_e}{2\sqrt{\alpha(t-\tau)}}\right] + \frac{1}{2} erf\left[\frac{T^i_R + x + 2nx_e}{2\sqrt{\alpha(t-\tau)}}\right] - \frac{1}{2} erf\left[\frac{T^i_L + x + 2nx_e}{2\sqrt{\alpha(t-\tau)}}\right] \right\} \tag{13}$$

$$T^i_{sy}(t-\tau) = \sum_{-\infty}^{\infty} \frac{1}{2\sqrt{\pi\alpha(t-\tau)}} \left\{ exp\left[\frac{(y^i - y + 2ny_e)^2}{4\alpha(t-\tau)}\right] + exp\left[\frac{(y^i + y + 2ny_e)^2}{4\alpha(t-\tau)}\right] \right\} \tag{14}$$

$$T^i_{sz}(t-\tau) = \sum_{-\infty}^{\infty} \frac{1}{2\sqrt{\pi\alpha(t-\tau)}} \left\{ exp\left[\frac{(z^i - z + 2nz_e)^2}{4\alpha(t-\tau)}\right] + exp\left[\frac{(z^i + z + 2nz_e)^2}{4\alpha(t-\tau)}\right] \right\} \tag{15}$$

$$L_{seg} = \frac{L}{N} \tag{16}$$

where, T^i_L, T^i_R, y^i, z^i are the location coordinates of ith segment in the 3D system. "erf" represents the error function defined in Eq. (17):

$$erf(x) = \frac{2}{\sqrt{\pi}} \int_0^x e^{-t^2} dt \tag{17}$$

Sub-systems coupling. The two sub-systems share the same conductive heat flux and the same temperature value at the midpoint at each segment. In sub-system #1, the temperature change at any location in Laplace domain can be expressed as:

$$\overline{\Delta T(x,y,z)} = \sum_{i=1}^{N} \overline{q^i} \cdot L\left[\frac{1}{\rho_r c_r} T^i_{sx}(t) T^i_{sy}(t) T^i_{sz}(t)\right] \tag{20}$$

Eq. (20) indicates that the temperature change value at the midpoint of each segment can be seen as a function with N unknown

variables, $\overline{q^i}(i\ from\ 1\ to\ N)$, with respect to the location (Eq. (21)). The source/sink function of each segment in Laplace domain, L[], could be numerically calculated by Chebyshev's Theorem.

$$\overline{\Delta T^i_{x_{mid-point}}} = f^i_{\#1}\left(\overline{q^1}, \overline{q^2}, \overline{q^3}, \ldots, \overline{q^i}, \ldots, \overline{q^N}\right),\ i\ from\ 1\ to\ N \tag{21}$$

In sub-system #2, the temperature value in Laplace domain at each interval can be derived from Eq. (19):

$$\begin{cases} \overline{\Delta T^i(x)} = \overline{\Delta T^i_{x=0}} \cdot e^{-\frac{s}{v}x} + \left(1 - e^{-\frac{s}{v}x}\right) \dfrac{\overline{q^i}}{sL_{seg}A\rho_f c_f},\ 0 \le x \le L_{seg} \\ \overline{\Delta T^i_{x=0}} = \overline{\Delta T^{i-1}_{x=L_{seg}}} \\ \overline{\Delta T^i_{x=L_{seg}}} = \overline{\Delta T^{i+1}_{x=0}} \\ \overline{\Delta T^1_{x=0}} = \dfrac{(T_r - T_{inlet})}{s} \end{cases} \tag{22}$$

As such, the temperature change at the mid-point of each segment is a function of location, and N unknown variables, $\overline{q^i}(i\ from\ 1\ to\ N)$.

$$\overline{\Delta T^i_{x_{mid-point}}} = f^i_{\#2}\left(\overline{q^1}, \overline{q^2}, \overline{q^3}, \ldots, \overline{q^i}, \ldots, \overline{q^N}\right),\ i\ from\ 1\ to\ N \tag{23}$$

Because the two sub-systems share the same temperature change at mid-point ($\overline{\Delta T^i_{x_{mid-point}}}$) and conductive heat flux value as the sink or source ($\overline{q^i}$) of each segment, N equations with N unknown variables can be generated and solved by Gaussian elimination (Eq. (24)). The mathematical calculations of source and sink functions, matrix computations, and following Laplace inverse process are realized by C++ coding in Microsoft® Visual Studio environment.

$$\begin{bmatrix} a_{11} & \cdots & a_{1N} \\ \vdots & \ddots & \vdots \\ a_{N1} & \cdots & a_{NN} \end{bmatrix} \cdot \begin{bmatrix} \overline{q_1} \\ \vdots \\ \overline{q_i} \\ \vdots \\ \overline{q_N} \end{bmatrix} = \begin{bmatrix} C_1 \\ \vdots \\ C_i \\ \vdots \\ C_N \end{bmatrix} \tag{24}$$

Stehfest inverse algorism. The solution from the matrix calculation is done in the Laplace domain. Stehfest numerical inversion (Eq. (25)) was applied to convert the solution into a real time domain [35].

$$f(t) = \frac{ln2}{t} \sum_{i=1}^{N_L} V_i F\left(\frac{ln2}{t} \cdot i\right) \tag{25}$$

where V_i can be calculated as following and N_L is either 6, 8, or 10; f(t) is the result in a real time domain; F() means the value in Laplace domain:

$$V_i = (-1)^{\left(\frac{N}{2}+i\right)} \sum_{k=\frac{i+1}{2}}^{min\left(i,\frac{N}{2}\right)} \left[\frac{k^{\frac{N}{2}+1} \cdot (2k)!}{\left(\frac{N}{2}-k\right)!k!(i-k)!(2k-i)!} \right] \tag{26}$$

Table 1
Parameters of cold-water injection case after unit converted from Ramey [26]].

Parameter	Value	Unit
Surface temperature	21.11	°C
Cold water temperature at inlet	14.72	°C
Geothermal gradient	0.01513	°C/m
Inner diameter	0.16	m
Length of the vertical well	1828.8	m
Water injection rate	8.732	kg/s
Thermal conductivity of water	0.5867	W/m/K
Density of water	990.65	kg/m^3
Specific heat capacity of fluid	4180	J/K/kg
Thermal conductivity of reservoir	2.423	W/m/K
Volumetric heat capacity of reservoir	2.352e6	J/K/m^3

4. Validation

There is no publicly available dataset for the validation of the proposed analytical methods. We use data presented in a cold-water injection case study by Ramey [26] to validate our models by comparing the computed results with the measured water temperature records. The cold water was injected through a vertical well in a reservoir with a pre-determined geothermal gradient. The water injection rate was maintained at a constant rate, and the temperature was measured along the wellbore after approximately 75 days. The parameters of reservoir and operation are listed in Table 1, and the results are shown in Fig. 7.

Fig. 7 presents a comparison of temperatures measured along the vertical wellbore with temperatures computed by Ramey's method and the two proposed analytical methods. The temperatures calculated from this study fit very well with Ramey's work. And the computed value was within 0.83 °C of the measured temperatures, which shows good application of this work on the heat transfer evaluation.

5. Results

An application example case of a closed-loop system defined by model parameters in Table 2 was used for developing a general

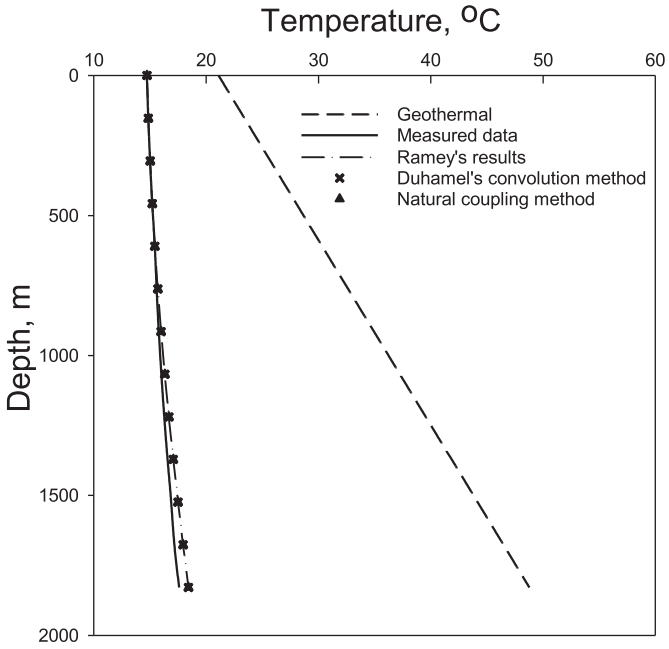

Fig. 7. Measured and computed temperature for a cold-water injection well.

Table 2
Parameters of reservoir and the closed loop well system used in the application example case.

Parameter	Symbol	Value	Unit
Reservoir temperature	T_r	150	°C
Length lateral	L	4000	m
Flow rate per lateral	q_f	20	m^3/hr
Inner diameter lateral	D	0.156	m
Inlet temperature	T_{inlet}	60	°C
Density of fluid	ρ_f	1000	kg/m^3
Specific heat capacity of fluid	c_f	4180	J/K/kg
Thermal conductivity of rock	λ	3.5	W/m/K
Density of rock	ρ_r	2500	kg/m^3
Specific heat capacity of rock	c_r	1100	J/K/kg
Segment length used in Natural Coupling Method	L_{seg}	100	m

understanding of heat production performance and for comparison with our two analytical methods. In this example, a 4000 m closed-loop system is completed in a reservoir layer with 3.5 W/m/K thermal conductivity and at 150 °C. The temperature at the end of lateral wellbore can been seen as the outlet temperature of the working fluid, if heat exchange is neglected in the vertical wellbore.

The outlet temperatures at the end of horizontal wellbore, calculated over 30 years by the two methods, exhibits good agreement as shown in Fig. 8. The outlet temperature drops dramatically from the reservoir temperature (150 °C) to 108 °C after the first year. The temperature continues to decline to 100 °C over the remaining years. As a result, this closed-loop system can provide a relatively stable energy production with fluids temperature over 100 °C on a 30 year lifespan. This maintained outlet temperature results from the heat balance between heat produced out for power generation and the heat loss from the cooled region near the wellbore (Fig. 9).

The Natural Coupling Method has been applied to show the heat transfer equivalent. The cumulative heat amount produced by fluid, Q_o, and heat loss from the reservoir, Q_r, can be expressed as:

$$Q_o = \int_0^t (T_{outlet} - T_{inlet}) \cdot \rho_f c_f \cdot q_f dt \tag{27}$$

$$Q_r = \iiint (T_r - T_{ave}) \cdot \rho_r c_r dx dy dz \tag{28}$$

Two cumulative heat amounts have been plotted over 30 years in Fig. 10. The two results clearly match, which shows highly accurate calculation of the proposed method in this study. The cumulative heat extracted from a thermal reservoir increases with the projects operating time, and it will reach 9.23e5 GJ at the end of 30 years.

6. Discussion

The thermal production efficiency and performance of a closed-loop system depends on many factors. These factors come from the nature of the reservoir, such as the thermal conductivity and temperature, and the operation variables such as the working fluids circulation rate, length of the lateral wellbore, and number and spacing of laterals. Sometimes, these factors will affect the thermal energy production performance together.

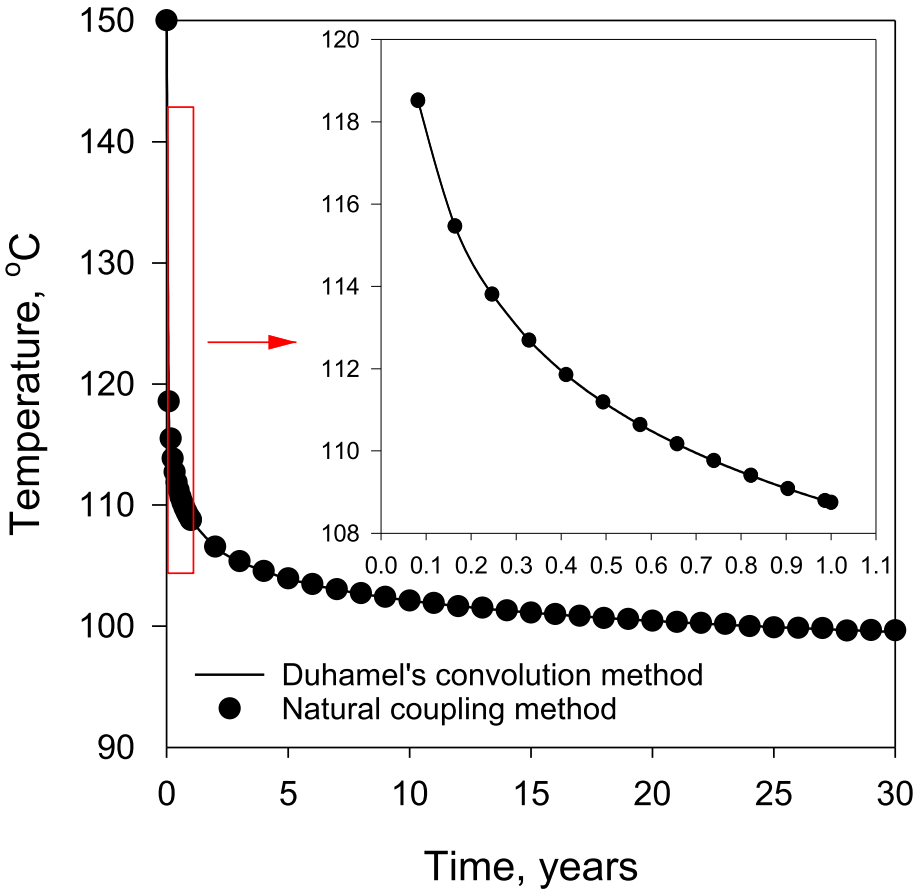

Fig. 8. The comparison plot of results from the two methods proposed in this study.

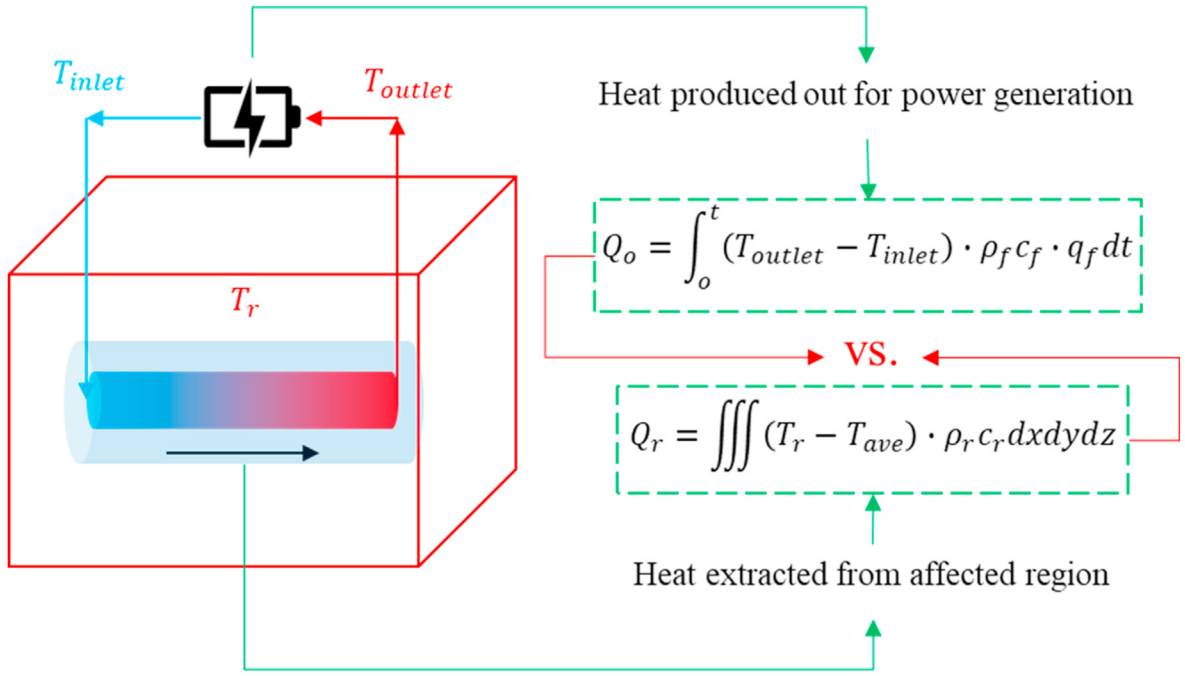

Fig. 9. Schematic diagram of the heat balance between heat production by hot working fluid cooling down and heat loss from affected reservoir region.

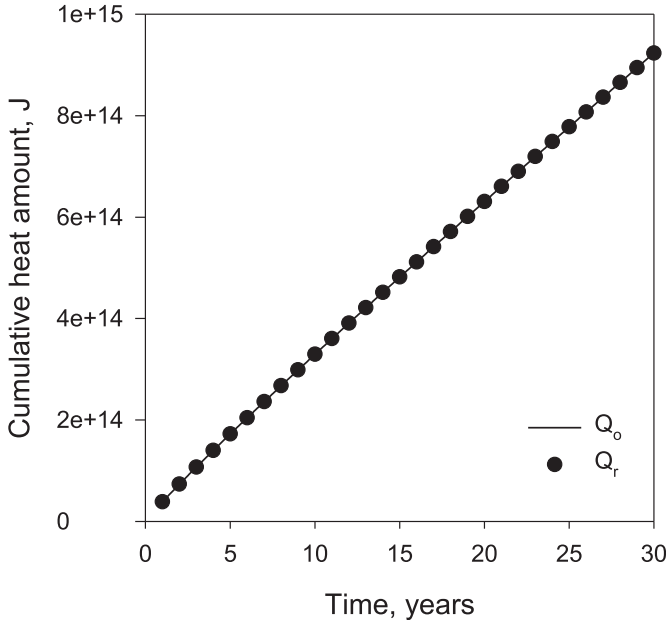

Fig. 10. Results of cumulative produced heat amount (Q_o) and heat loss from affected reservoir region (Q_r).

Thermal conductivity. Reservoir thermal conductivity is the most important parameter to evaluate the feasibility of a closed-loop geothermal system to recover energy from a thermal reservoir. Because the lateral wellbore is in a closed loop and there is no fluid communication between the reservoir and wellbore, heat conduction is the only heat transfer mechanism in a closed-loop system. Reservoir thermal conductivity is highly related to the rock solidity (the ratio of the volume of solids to the bulk volume) and local temperature. Usually, higher rock solidity and lower reservoir temperature will result in higher thermal conductivity [36]. Solidity and temperature also affect the drilling cost and efficiency of energy conversion to electric power. As such, it is crucial to determine the optimum production layer for a closed-loop system. For sedimentary basins, thermal conductivity usually ranges from 2 to 5 W/m/K [37], and among common minerals, quartz has the highest thermal conductivity, around 7 W/m/K. Here we used a sensitive analysis of thermal conductivity ranging from 1 to 7 W/m/K to test the application example in this study.

Outlet temperatures, under various reservoir thermal conductivities, are plotted in Fig. 11. Results show outlet temperature over a 30 year period is clearly dependent on thermal conductivity. The highest thermal conductivity, 7 W/m/K, yields the highest outlet temperature of slightly over 120 °C at the end of 30 years, while the lowest thermal conductivity, 1 W/m/K results in the lowest temperature of about 75 °C, or half of the original reservoir temperature. The drop in outlet temperature with decreasing thermal conductivity is nonlinear. When thermal conductivity is lower than 4 W/m/K, the difference in outlet temperature between adjacent time series become more significant (Fig. 11). As thermal conductivity of most sedimentary sequences is less than 4 W/m/K in sedimentary basins, targeting of higher thermal conductivity layers for installation of the horizontal leg is important for project success.

Initial local reservoir temperature. Target reservoir temperature is one of the most important parameters to assess if a thermal reservoir is suitable for commercialized electricity power generation as compared to direct heat utilization. Three different local reservoir temperature, T_r, have been studied to analyze the outlet temperature performance and the corresponding temperature difference between inlet and outlet temperature (Fig. 12), to help understand heat harvesting efficiency.

In general, higher local temperatures will result in higher outlet temperatures of the working fluids. A reservoir rock at 200 °C will produce over 120 °C fluids, while a 100 °C reservoir can only produce fluids around 78 °C after 30 years of operation. In terms of the temperature difference between inlet and outlet temperature, higher local reservoir temperatures contribute to greater heat harvesting, which means a higher temperature reservoir will also give better heat recovery efficiency. While the local reservoir

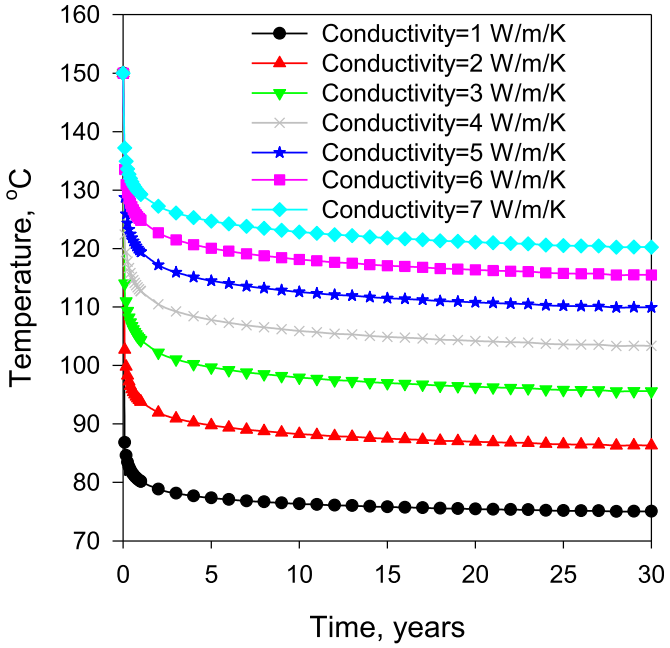

Fig. 11. Outlet temperature profiles over 30 years under various reservoir thermal conductivities.

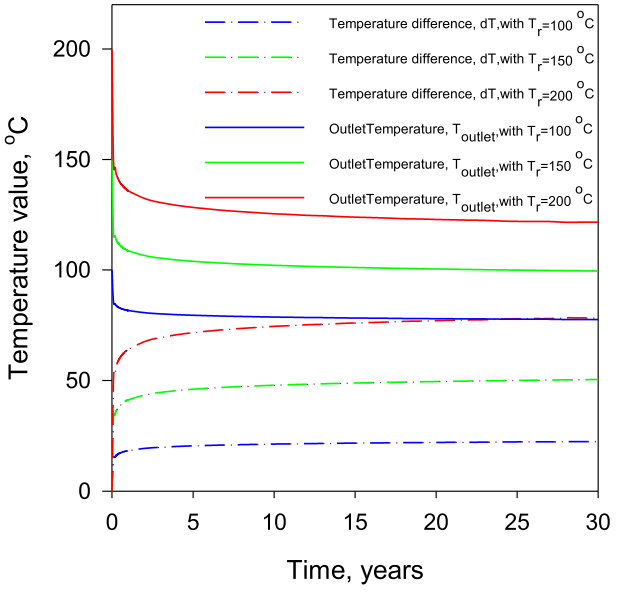

Fig. 12. Outlet temperature and temperature difference between outlet and inlet results under three different local reservoir temperatures.

temperature increases with depth, thermal conductivity varies as a function of lithology (Fig. 13). So, optimization on both local temperature and thermal conductivity is critical for closed-loop geothermal energy production project design. A shallower and cooler layer with higher thermal conductivity may produce more energy than a deeper hotter layer.

Residence time. In the project design phase, the length of the horizontal wellbore is one of the key parameters that affect the overall heat extraction efficiency. Generally, a longer horizontal wellbore will allow the working fluid to have more contact area with the thermal reservoir. However, increasing the length of the lateral part of the wellbore will also increase the difficulty of

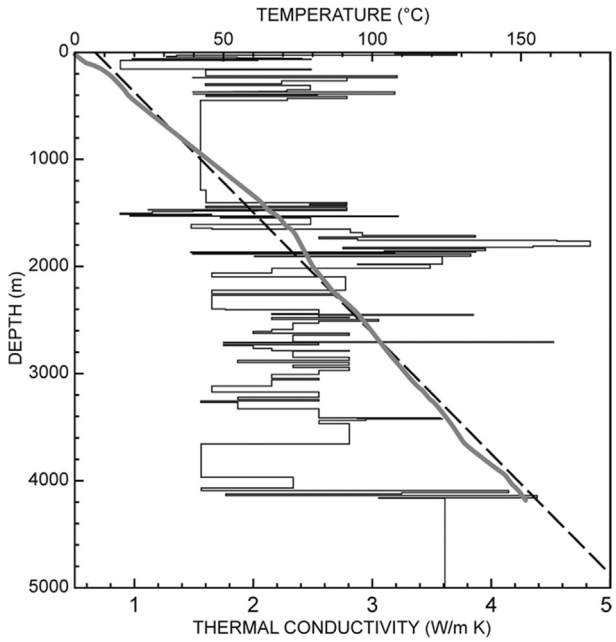

Fig. 13. Example of the variation of thermal conductivity with depth in northeaster British Columbia (in the NW part of the WCSB), and the related thermal gradient variation, from Majorowicz et al. [37].

drilling and completion. The associated higher capital cost will also increase the risk. From a geological perspective, a longer wellbore may exceed the reservoir boundary or increase the possibility of significant reservoir heterogeneity, which will all increase the uncertainty of the project. Whereas, from the engineering perspective, increasing wellbore length will also bring unexpected problems related to wellbore integrity. On the other hand, the fluid velocity within a horizontal wellbore also affects the heat extraction performance. Higher fluid velocity will reduce the contact time of fluid with the thermal reservoir, lowering the outlet temperature. However, a lower velocity may not meet the required flow rate for heat production. As such, optimized lateral length and fluid velocity in the horizontal section need to be considered carefully in the project design phase.

It is interesting to note that the lateral length and fluid velocity can compensate for each other's effect on the outlet temperature as shown graphically in Fig. 14 and mathematically in the Duhamel's convolution model of Eq. (11). The ratio L/v has a dimension of time and the physical meaning is the required time of the working fluid to move through the lateral wellbore. This time, denoted as t*, is defined as residence time in the horizontal wellbore with a mathematical form as:

$$t^* = \frac{L}{v} \tag{29}$$

A larger residence time means more time for fluid contact with the thermal reservoir, increasing heat gain. Fig. 15 displays the fluid outlet temperatures for various residence times, demonstrating how residence time affects heat extraction performance. In Fig. 15, residence time of the application example case in this study is 3.82 h (black). When residence time is 4.78 h (red), the outlet temperature is higher over 30 years. When residence time is smaller (e.g., 2.87 h) the outlet temperature is lower. The difference between the adjacent series could reach up to 10 °C. However, larger residence times requires larger lateral length or lower fluid velocity. A project needs to consider carefully this value to optimise

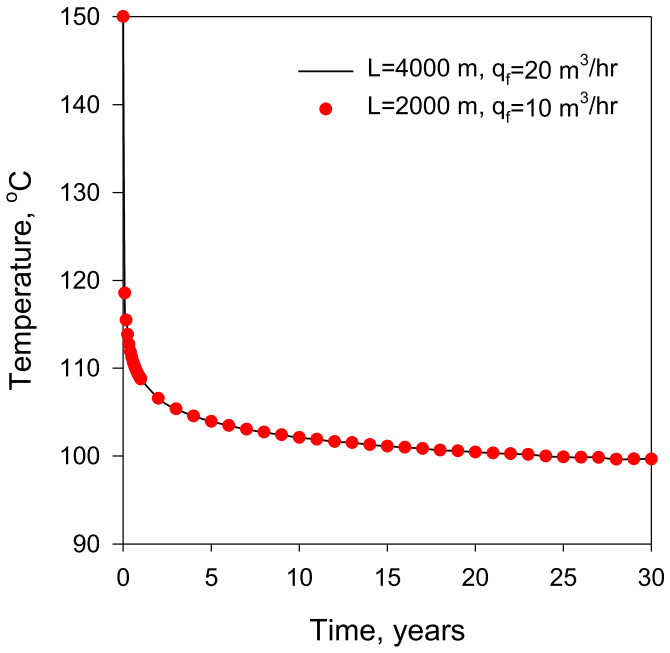

Fig. 14. Outlet temperature profiles over 30 years under different lateral lengths and flow rates.

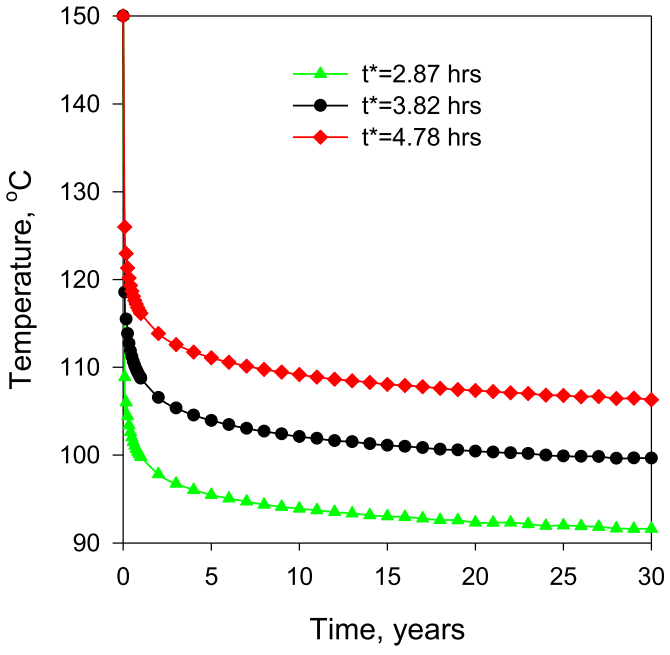

Fig. 15. Outlet temperature profiles over 30 years under various residence times.

heat extraction performance based on the fundamental geology setting.

Multilateral well interference. Closed-loop geothermal energy recovery technology needs multiple wells to extract enough thermal energy to meet the requirement of electricity power generation; the structure and design of multilateral wells will also significantly affect heat loss reduction in the vertical production wellbore, as discussed in the next section.

In a multilateral development, each transient heat drainage area expands with time. When the drainage areas of adjacent wellbores merge, the heat recovery will be affected by lowering the outlet temperature based on the principal of superposition. The time and degree of the temperature drop depends on well spacing, reservoir thermal conductivity, and other system parameters such as heterogeneity of the reservoir. In order to eliminate or minimize the interference effect on a closed-loop geothermal project, well interference needs to considered in the design phase.

Fig. 16 compares the outlet temperature over 30 years under various lateral spacing of a two-lateral well configuration. The temperature profile from a single lateral configuration was also plotted in the figure for reference. The single lateral case has the highest outlet temperature since there is no other well competing with it. The case with 25 m spacing is the first to deviate from the single lateral case, as a drop in temperature, over the 30-year production period. The cases with 50 m and 75 m spacing deviate from the single lateral case later in time. The smallest spacing also displays the most significant well interference. The difference could be 5 °C for each lateral, and the overall heat extraction efficiency could be significantly reduced by having horizontal leg spacing too close. In this study, 75 m would provide the minimum well interference effect. However, larger spacing distance means higher drilling costs and technical difficulty. Detailed simulation and sensitive analysis are needed for specific project design and optimization.

Another important factor affecting lateral-interference is the reservoir thermal conductivity. A higher thermal conductivity means a greater distance of thermal effect on reservoir. In the oil and gas industry, the definition of radius of investigation helps to evaluate how fast a reservoir can transfer pressure changes. Similarly, in the geothermal industry, the radius of investigation could be defined as:

$$r_i = \sqrt{\frac{4\lambda t}{\rho_r c_r}} \tag{30}$$

Higher thermal conductivity will result in a greater area of temperature change at any given time. So, a higher thermal conductivity will lead to earlier and more significant well interference.

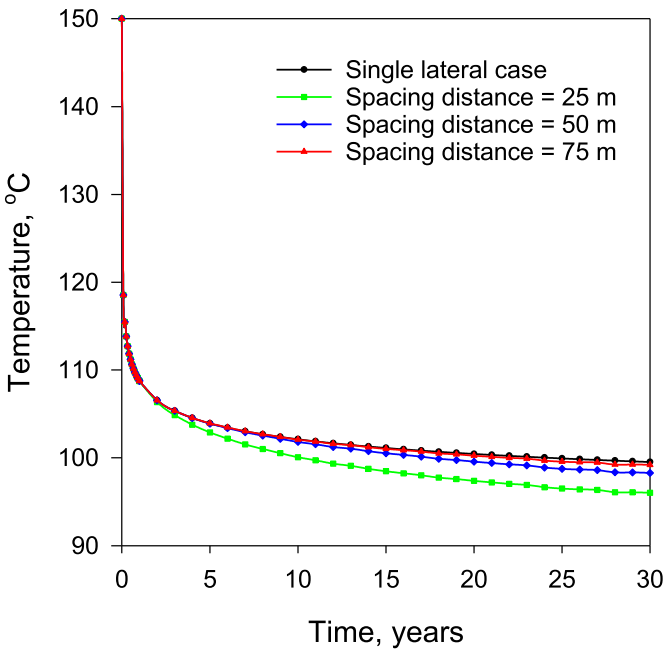

Fig. 16. Outlet temperature profiles of a two-lateral instalment with different horizontal spacing.

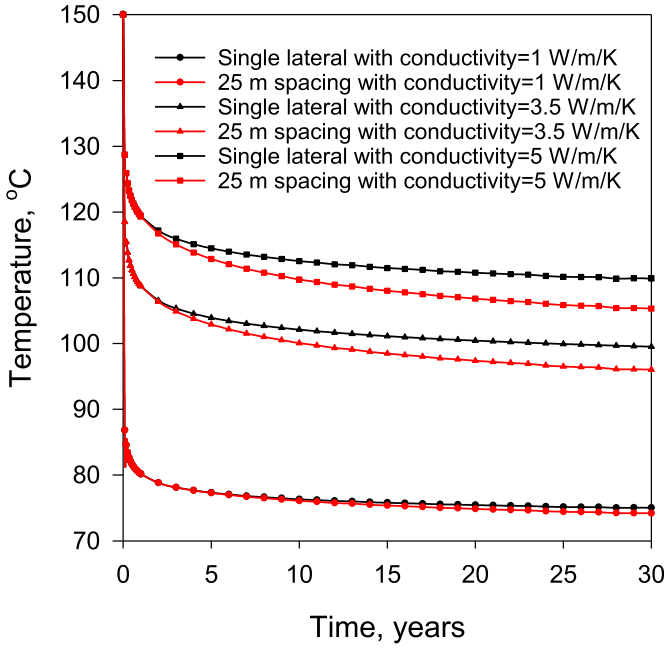

Fig. 17. Outlet temperature profiles of a two-lateral case of 25 m spacing with different reservoir thermal conductivities.

Outlet temperature profiles for three different reservoir thermal conductivities for both single-lateral and double-lateral well configurations are plotted in Fig. 17. The reservoir with 5 W/m/K conductivity has the highest outlet temperature, but with the earliest and strongest well interference effect. When the thermal conductivity is low, 1 W/m/K, the well interference could be neglected due to a slow heat transfer mechanism.

When the number of laterals in a well pad is more than two, the level of well interference for each lateral is different. To study the heating performance of each lateral, the temperature profiles at the end of the horizontal part of each lateral need to be determined. Fig. 18 shows the temperature at the end of each lateral for a 10-lateral multilateral well pad over 30 years under three different reservoir thermal conductivities. In the first several years, the temperature at the end of each lateral shows the same value, because there is no well interference or limited interference at that time. However, later in time, the temperature profiles of the middle laterals are lower than the wells near the edge. That is because the laterals in the middle location experience the most significant well interference effect and the heat extraction efficiency is reduced by surrounding laterals. Higher reservoir thermal conductivities will result in more significant well interference and larger temperature drops. Large temperature differences between laterals may lead to less heat extraction efficiency and its final efficiency of transition to electricity power. Operation optimization can minimize the temperature difference of each lateral in the design phase. For example, variable spacing distances could be applied to multilateral well pad, so that the temperature of middle laterals will be closer to the others.

Heat exchange in vertical wellbores. The working fluid transported through vertical wellbores in injection and production well will lose or gain heat depending on the temperature variation encountered. This amount of heat could affect the overall heat extraction performance. The application example in this study is used to examine this influence. A typical geothermal gradient is assumed as shown in Fig. 19. The surface temperature is assumed to be 5 °C, while the target reservoir has a temperature of 150 °C at 3000 m depth. The temperature increases linearly with depth. The working fluid has a temperature of 60 °C when injected at the surface and will be heated along the 4000 m horizontal wellbore. Heated fluid will be then transported to surface by a 3000 m production well. The overall process is illustrated in Fig. 19 and the parameters of the system are listed in Table 3.

In the thermal domain, heat transfer between the inner wellbore and outside reservoir occurs where there is a temperature difference. There are three main parts of the system having heat transfer with the outside reservoir (Fig. 20). The first part is the vertical injection wellbore. Because the inlet temperature of the working fluid at the surface is 60 °C, which is higher than the temperature of the stratigraphic interval above a certain depth, there will be some heat loss from the downward moving working fluid. When fluids move to a depth where rock temperature is higher than that of downward fluid, it starts to gain heat from surrounding rocks. Through the entire lateral wellbore, the working fluid continuously gains heat. At the end of lateral wellbore, heated fluids from multilaterals merge and flow upwards through the vertical production well. The fluid temperature reaches the maximum at the base of the vertical production well (Fig. 20).

In this study, we applied Duhamel's Convolution Method to calculate the heat transfer in vertical sections of the wellbore with an assumption of no well interference. While for heat transfer modeling in the laterals, the Natural Coupling Method was applied to deal with potential multilateral well interference and the complex geological conditions. Three modeling parts of the system were integrated with two connecting points (Fig. 20). While the analytical method helped generate more accurate results.

Firstly, a simple single lateral case was studied to see how heat exchange in vertical wellbore affects the overall energy extraction performance. Fig. 21 shows the time series of temperature variations throughout the closed-loop system over 30 years of operation. The first and last 3000 m of the system are the vertical injection and production segments. The 4000 m in the middle is the horizontal part. In general, the temperature decreases from 60 °C at the surface and increases from around 1000 m vertical depth. At the end of the vertical injection section in the first year, the temperature reaches 66 °C. The fluid temperature at the end of lateral reaches 111 °C. The temperature of the fluids continues to increase in the vertical production section until the temperature reaches about the same level of the surrounding rocks outside of the wellbore. The temperature of working fluid decreases to 99 °C at the outlet. As a result, the temperature difference between the end of lateral and outlet of production well could be 12 °C, suggesting that the working fluids may lose significant heat in the vertical production section in a single lateral setting.

The results from 10 multilaterals are plotted in Fig. 22. High flow rate fluids (10 times in mass) are injected through the vertical injection well to the wellbore downhole. At the first connecting point, the fluids are separated into 10 laterals and flow towards the production segment. At the end of the laterals, the heated fluids have a temperature of 109 °C and merge together in the bottom of the production well. There is a much larger upward convective flow mass in the vertical wellbore and conductive heat loss crossing the wall of the wellbore is limited. As a result, the temperature of the working fluid is 107 °C at the outlet, with a loss of 2 °C in the upward journey. For the same reason, the temperature increases only 0.5 °C at the end of injection section. The multilateral well configuration with much higher flow rates or larger flow mass in the upward vertical section can reduce heat loss.

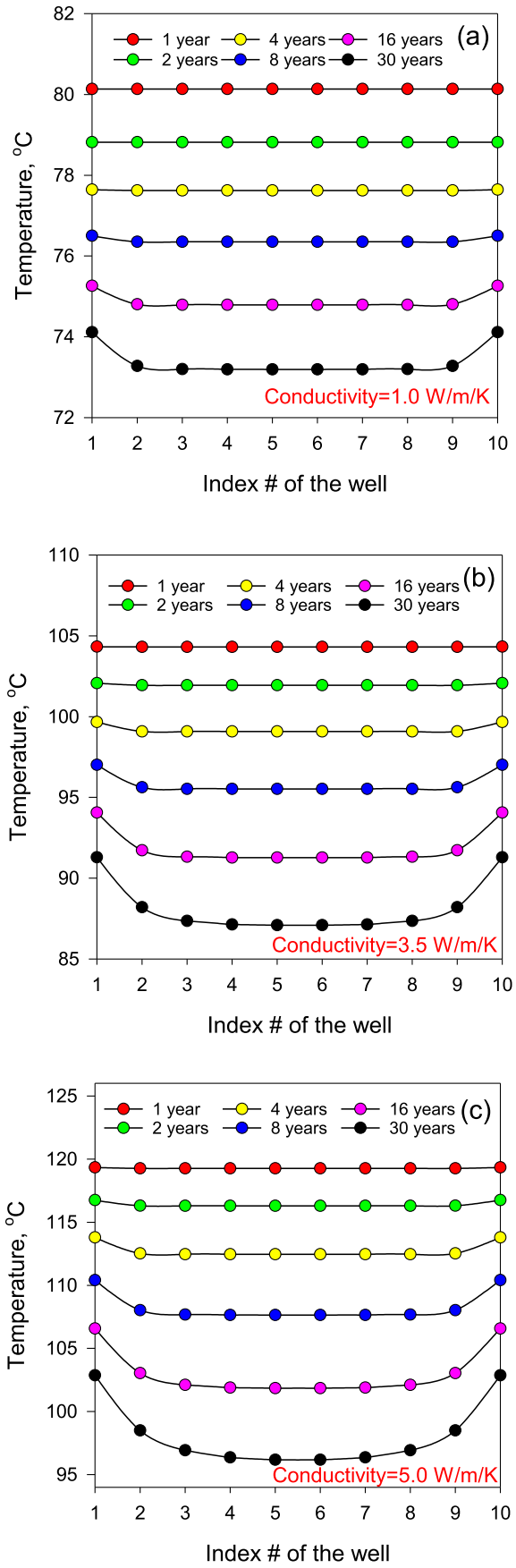

Thermal production. The most important indicator of a successful geothermal energy project is the thermal production capacity. We use the 10 lateral system to calculate the long-term thermal energy production. The temperature difference between the outlet and inlet multiplied by the volumetric heat capacity and flow rate yields the heat duty. The corresponding cumulative thermal production with time is plotted in Fig. 23. This 10-laterals system with application example reservoir and well parameters generates 11 MW thermal heat energy in the early production period, drops to 10 MW at the 6th year, and remains above 9 MW for the rest of the period. The total heat production at 30 years will reach 2.5e9 kWh. The power consumption by pump at the injector is limited due to the utilization of the thermosiphon effect of the working fluid. Because the temperature at the outlet decreases gradually, the thermosiphon effect will reduce overtime. Assume the pressure is maintained at 1300 kPa at the injector and the roughly total pressure drop of 700 kPa at the end of 30 years, the pumping power of less than 45.75 kW with 85% pump efficiency is needed over the 30 years. This is just a hint of pump energy needed, and the accurate estimation of pump power consumption needs to consider the pipe friction, flow rate, diameter changes, elbows, and pressure losses due to surface piping and equipment system [38]. As a result, this horizontal closed-loop geothermal project could provide stable and acceptable heat production. However, the conditions to have such outcome are critical. Our base case uses 10 lateral wells of 4000 m long, and, most importantly, 3.5 W/m/K or higher reservoir thermal conductivity and 150 °C or higher reservoir temperature.

7. Conclusions

In this study, two novel analytical methods were proposed to evaluate the closed-loop system. Duhamel's convolution method used in oil and gas industry was applied in modeling of a single lateral closed-loop geothermal energy recovery system. For more complicated cases such as multilateral wells, and heterogeneous and bounded reservoirs, the natural coupling analytical method was applied to deal with the complexity of the system to help better understand heat transfer behaviour and interaction between the working fluid and reservoir in a closed-loop system.

An application example case with typical geothermal reservoir properties and closed-loop parameters was examined in this study. The outlet temperature profiles over 30 years from two different approaches are comparable with high accuracy. The heat balance check between energy production and heat loss from the reservoir helps validate the proposed methods for the closed-loop geothermal recovery technology. The application of the methods to the application example case in this study suggests that closed-loop system provides a reasonable stable heat production.

A sensitivity study suggests reservoir thermal conductivity, determining the efficiency of heat transfer from reservoir to the working fluid, is the most important parameter of the system to evaluate whether a reservoir is suitable for a closed-loop geothermal energy recovery project. Well interference in a multilateral configuration could be eliminated or reduced by increasing well spacing. Higher reservoir thermal conductivity will also lead to earlier well interference and larger temperature drops through time. However, the lateral length and flow rate compensate for each other on overall heat extraction performance. For a given thermal reservoir, optimizing the operational parameters, such as length,

Fig. 18. Temperatures after 30 years for a 10 lateral well system under 25 m well spacing with 1 W/m/K thermal conductivity a); 3.5 W/m/K thermal conductivity b); and 5 W/m/K thermal conductivity c).

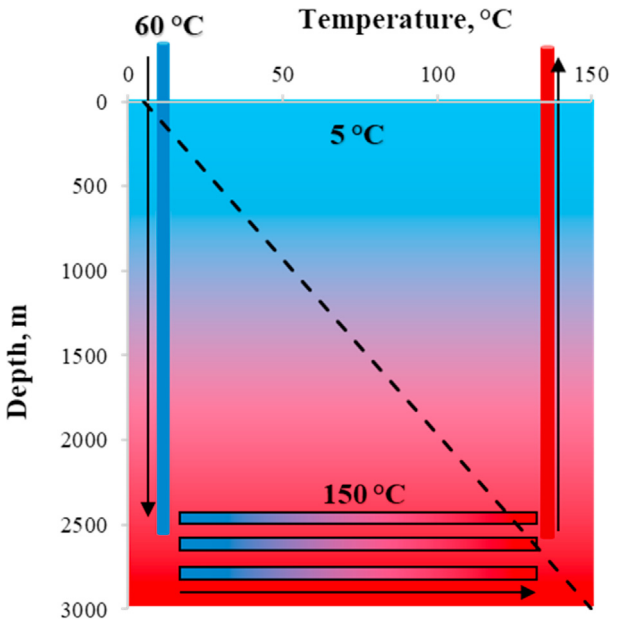

Fig. 19. Flow diagram of the working fluid in a closed-loop geothermal energy recovery system with consideration of geothermal gradient existing (black dashed line).

Table 3
Parameters of reservoir and well system used in this case of studying heat exchange in vertical wellbores.

Parameter	Symbol	Value	Unit
Depth	h	3000	m
Length lateral	L	4000	m
Reservoir temperature	T_r	150	°C
Surface temperature	T_s	5	°C
Flow rate per lateral	q_f	20	m^3/hr
Number of laterals	N_l	10	
Inner diameter lateral	D_l	0.156	m
Inner diameter of vertical wellbore	D_v	0.21	m
Inlet temperature at the surface	T_{inlet}	60	°C
Density of fluid	ρ_f	1000	kg/m^3
Specific heat capacity of fluid	c_f	4180	J/K/kg
Rock thermal conductivity of lateral part	λ_l	3.5	W/m/K
Rock thermal conductivity of vertical part	λ_v	2.0	W/m/K
Density of rock	ρ_r	2500	kg/m^3
Specific heat capacity of rock	c_r	1100	J/K/kg
Segment length used in Natural Coupling Method	L_{seg}	100	m

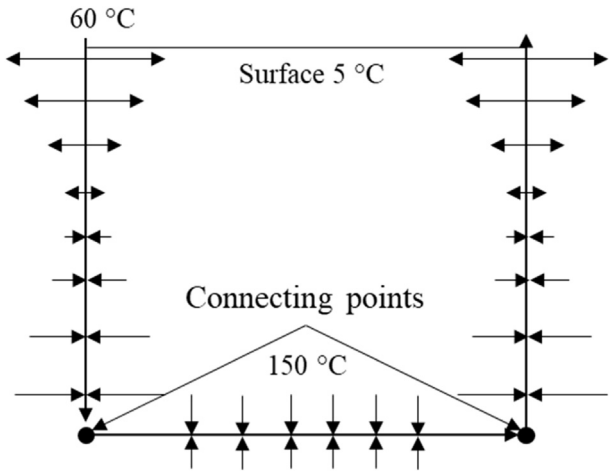

Fig. 20. Schematic diagram of conductive heat transfer between total wellbore and outside reservoir in closed-loop geothermal energy recovery system with consideration of the geothermal gradient.

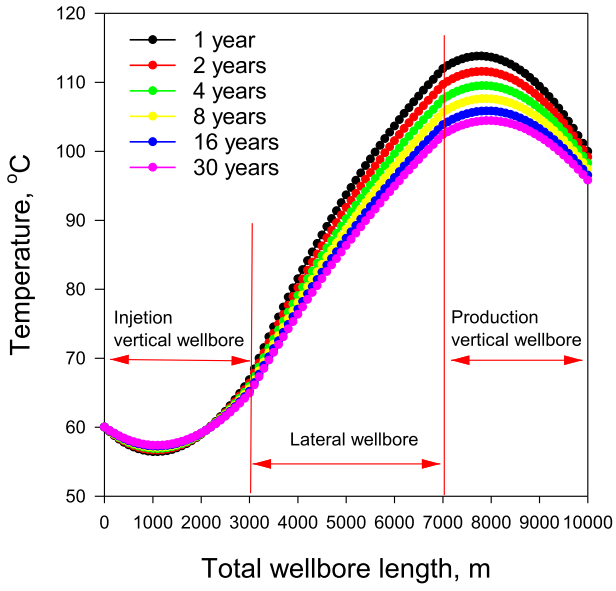

Fig. 21. Working fluid temperature variation in a single lateral wellbore.

spacing, flow rate and number of laterals in the project design phase can greatly increase efficiency.

The heat exchange effect in vertical injection and production sections is minimal in a 10-multilateral closed-loop configuration. With the application example case, the closed-loop geothermal energy recovery technology could provide 9–11 MW stable heat production over 30-years of operation.

Our results show that a deep closed loop system can effectively produce energy over long time periods under suitable geological settings regarding thermal gradient and thermal conductivity. Both of these parameters are easier to determine or already known in many petroleum basins. Our model was based on average conditions and the resultant outlet temperature may be more suitable for district heating rather than power generation. That being said, higher temperature target reservoirs would be capable of producing higher outlet temperatures with potential for power generation. We have restricted our assessment to the thermodynamic viability of this technology. Demonstration projects have proven that the drilling technology is viable. We have not assessed the economics of this technology, which will in large part be related to drilling costs. Overall, this technology removes the need of permeable zones which conventional geothermal production methods require and avoids artificial fracturing in an enhanced geothermal system, thereby providing an alternative solution for many high enthalpy geothermal projects. As well, a closed-loop system eliminates challenges related to production of geothermal fluids, including scaling and environmental risks. Further research can greatly expand the deployment of geothermal development to support the transition to clean energy resources.

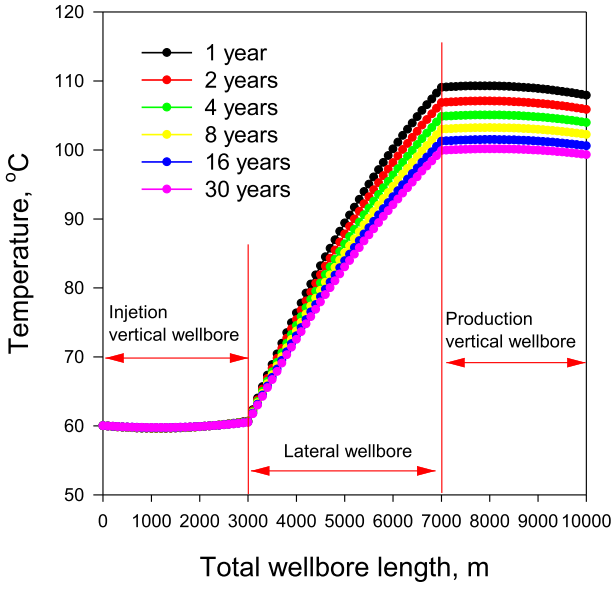

Fig. 22. Temperature profiles along total wellbore length of 10-laterals case.

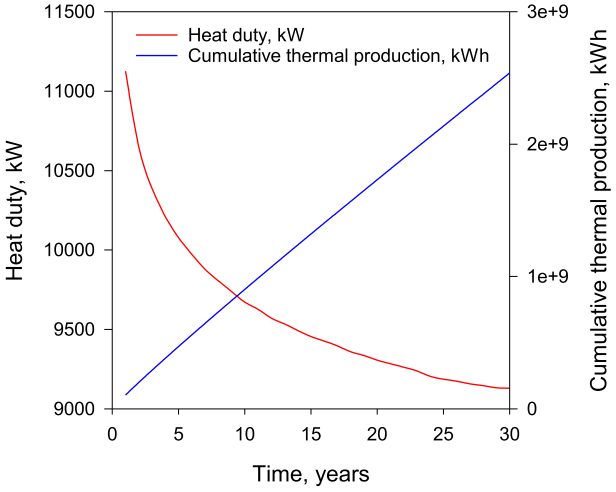

Fig. 23. Heat duty and cumulative thermal production profiles over 30 years of 10-laterals case.

CRediT authorship contribution statement

Wanju Yuan: Methodology, Formal analysis, Software, Writing – original draft. **Zhuoheng Chen:** Conceptualization, Supervision, Writing – review & editing, Funding acquisition. **Stephen E. Grasby:** Conceptualization, Writing – review & editing. **Edward Little:** Project administration, Writing – review & editing.

Declaration of competing interest

The authors declare that they have no known competing financial interests or personal relationships that could have appeared to influence the work reported in this paper.

Acknowledgements

This work originated as an independent evaluation of deep closed-loop system and is an output of the Geoscience for New Energy Supply (GNES) Program of Natural Resources Canada. Office of Energy Research and Development (OERD) provided funding for this study. The authors appreciate discussions with Eavor on the basic principals, however the modeling work conducted here was completely independent and any errors or omissions are the authors alone. The authors also thank our internal reviewer, Heather King, and four anonymous external reviewers for their constructive comments and suggestions on this paper. This paper has been assigned NRCan contribution number: 20200775.

References

[1] International Energy Agency (IEA), Renewables 2018: Market Analysis and Forecast from 2018 to 2023, 2018. https://www.iea.org/renewables2018/.
[2] D. Gielen, F. Boshell, D. Saygin, M.D. Bazilian, N. Wagner, R. Gorini, The role of renewable energy in the global energy transformation, Energy Strategy Reviews 24 (2019) 38–50, https://doi.org/10.1016/j.esr.2019.01.006.
[3] S. Schumacher, R. Pierau, W. Wirth, Probability of success studies for geothermal projects in clastic reservoirs: from subsurface data to geological risk analysis, Geothermics 83 (2020) 375–6505, https://doi.org/10.1016/j.geothermics.2019.101725.
[4] M. Abbasi, N. Khazali, M. Shari, Analytical model for convection-conduction heat transfer during water injection in fractured geothermal reservoirs with variable rock matrix block size, Geothermics 69 (April) (2017) 1–14, https://doi.org/10.1016/j.geothermics.2017.04.002.
[5] Y. Zhang, C. Yu, G. Li, X. Guo, G. Wang, Y. Shi, C. Peng, Y. Tan, Performance analysis of a downhole coaxial heat exchanger geothermal system with various working fluids, Appl. Therm. Eng. 163 (September) (2019), 114317, https://doi.org/10.1016/j.applthermaleng.2019.114317.
[6] Greenfire Energy, GreenLoopTM technology overview, 2021. Available on the internet: https://www.greenfireenergy.com/greenloop-technology/.
[7] P.B. Umwelt, Investigations on the Improvement of the Energy Output of a Closed Loop Geothermal System (CLGS), Technical University of Berlin, 2008.
[8] GeothermamEx Inc, Report on the South Meager Geothermal Resource British Columbia, Canada, for Western Geopower Corp, 2004, p. 156p.
[9] S.E. Grasby, D.M. Allen, S. Bell, Z. Chen, G. Ferguson, A. Jessop, M. Kelman, M. Ko, J. Majorowicz, M. Moore, J. Raymond, R. Therrien, Geothermal energy resource potential of Canada, Geological Survey of Canada, Open File 6914 (2011) 322.
[10] J. Majorowicz, S.E. Grasby, High potential regions for enhanced geothermal systems in Canada, Nat. Resour. Res. 19 (2010) 177–188.
[11] J. Majorowicz, S.E. Grasby, Geothermal energy for northern Canada – is it economic? Nat. Resour. Res. 23 (2014) 159–173.
[12] J. Majorowicz, S.E. Grasby, Deep geothermal energy in Canadian sedimentary basins vs. fossil based energy we try to replace – exergy [KJ/Kg] compared, Renew. Energy 141 (2019) 259–277.
[13] S. Weides, J. Majorowicz, Implications of spatial variability in heat flow for geothermal resource evaluation in large foreland basins: the case of the western Canada sedimentary basin, Energy 7 (2014) 2573–2594, 2014.
[14] S.B. Mahbaz, A.R. Dehghani-sanij, M.B. Dusseault, J.S. Nathwani, Enhanced and integrated geothermal systems for sustainable development of Canada' s northern communities, Sustainable Energy Technologies and Assessments 37 (2020), 100565, https://doi.org/10.1016/j.seta.2019.100565.
[15] Deep Earth Energy Production, About DEEP, 2021. Available on the Internet: https://deepcorp.ca/.
[16] Eavor Technologies Inc, Available on the Internet: https://eavor.com/about/technology, 2021.
[17] C. Hickson, M. Kumataka, P. Akto, D. Cotterill, D. Benoit, R. Eccles, K. Huang, M. Colombina, S. Collins, Alberta # 1: the Province's First Electrical Geothermal Project, vols. 1–13, 2020.
[18] H. Shao, P. Hein, A. Sachse, O. Kolditz, Geoenergy Modeling II, Springer International Publishing, 2016, https://doi.org/10.1007/978-3-319-45057-5.
[19] Z. Hu, T. Xu, B. Feng, Y. Yuan, F. Li, G. Feng, Z. Jiang, Thermal and fluid processes in a closed-loop geothermal system using CO_2 as a working fluid, Renew. Energy 154 (2020) 351–367, https://doi.org/10.1016/j.renene.2020.02.096, 2020.
[20] J.W. Tester, B.J. Anderson, A.S. Batchelor, D.D. Blackwell, R. DiPippo, The Future of Geothermal Energy - Impact of Enhanced Geothermal Systems (EGS) on the United States in the 21st Century, 0-615-13438-6, Massachusetts Institute of Technology, 2006. Available from: the Internet: www1.eere.energy.gov/geothermal/pdfs/future_geo_energy.pdf.
[21] M. Akhter, J. Mallams, X. Tang, A. Kazi, Y. Kao, S. Kumar, B. Tai, D. Antao, A. Palazollo, D. Staack, Shockwave and plasma accelerated rock cracking (SPARC) for hard rock drilling, in: Bulletin of the American Physical Society, 73rd Annual Gaseous Electronics Virtual Conference, 2020. October 5–9, 2020.
[22] J. Finger, D. Blankenship, Handbook of Best Practices for Geothermal Drilling, 2010. Sandia Report (SAND2010-6048), http://artikel-software.com/file/geothermal drilling handbook.pdf.
[23] Geothermal Engineering ltd., 2021. Available on the Internet: https://geothermalengineering.co.uk/united-downs/#.
[24] K. Huang, C. Hickson, D. Cotterill, Y. Champollion, Geothermal assessment of

target formations using recorded temperature measurements for the Alberta No. 1 geothermal project, Appl. Sci. 11 (2) (2021) 1–10, https://doi.org/10.3390/app11020608.
[25] M. Toews, "Method and Apparatus for Power Production" U. S. Patent Application No. 16/181,492, Filed on Nov. 6. 2018, 2019. Pub. No.: US 2019/0154101 A1. May 23.
[26] H.J. Ramey, Wellbore heat transmission, J. Petrol. Technol. (1962) 427–435.
[27] J. Hagoort, Ramey's Wellbore heat transmission revisited, SPE J. 9 (4) (2004) 465–474, https://doi.org/10.2118/87305-PA –441.
[28] H.S. Carslaw, J.C. Jaeger, Conduction of Heat in Solids, second ed., University Press, Oxford, 1959, p. 339. Oxford at the Clarendon Press.
[29] W.H. Press, S.A. Teukolsky, W.T. Vetterling, B.P. Flannery, Numerical recipes in C. The Art of Scientific Computing, second ed., Cambridge University Press, USA, 1992, ISBN 978-0-521-43108-8.
[30] G. Zhao, Modeling Complex Natural Fracture Network in Heterogeneous Tight Formations Using Semi-analytical Strategy, Society of Petroleum Engineers, 2013, https://doi.org/10.2118/167127-MS.
[31] G. Zhao, L. Xiao, C. Su, Z. Chen, K. Hu, Model-based type curves and their applications for horizontal wells with multi-staged hydraulic fractures, Journal of Canadian Energy Technology Innovation (CETI) 2 (3) (2016) 29–43. January 2016.
[32] L. Xiao, G. Zhao, H. Qing, A compatible boundary element approach with geologic modeling techniques to model transient fluid flow in heterogeneous systems, J. Petrol. Sci. Eng. 151 (2017a) 318–329, https://doi.org/10.1016/j.petrol.2017.01.011, 2017.
[33] L. Xiao, G. Zhao, H. Qing, Depletion-induced stress change in a hydraulically bounded reservoir with multistage fractured horizontal wells, J. Nat. Gas Sci. Eng. 45 (2017b) 272–290, https://doi.org/10.1016/j.jngse.2017.05.003, 2017.
[34] C. Su, Semi-analytical Modeling of Fluid Flow in and Formation Evaluation of Unconventional Reservoir Using Boundary Integration Strategies, PhD Dissertation, Faculty of Graduate Study and Research, University of Regina, 2018. July, 2018.
[35] H. Stehfest, Numerical inversion of Laplace transforms, Commun. ACM 13 (1) (1970) 47, 1970.
[36] E.C. Robertson, Thermal Properties of Rocks, vol. 88, US Department of the Interior: Geological Survey, 1988.
[37] J.A. Majorowicz, F.W. Jones, A.M. Jessop, Preliminary geothermics of the sedimentary basins in the Yukon and Northwest territories (60-70 degrees north) - estimates from petroleum bottom-hole temperature data, Bull. Can. Petrol. Geol. 36 (1988) 39–51.
[38] S. Schulz, Investigations on the Improvement of the Energy Output of a Closed Loop Geothermal System (CLGS), PhD Dissertation, Faculty of Planning, Building, Environment, Technical University of Berlin, 2008, 2008.
[39] C.M. Oldenburg, L. Pan, M.P. Muir, A.D. Eastman, B.S. Huggins, Numerical Simulation of Critical Factors Controlling Heat Extraction from Geothermal Systems Using a Closed-Loop Heat Exchange Method, Lawrence Berkeley National Laboratory Recent Work, 2019. Permalink: https://escholarship.org/uc/item/4nj3s9ws.
[40] G. Zhao, Reservoir modeling method." U. S. Patent provisional application No. 61/226, 197, filed on july 16, 2009. Pub. No.: US 2011/0015909 A1. January 20, 2011, US Patent No 8 (2012) 275, 593, granted on Sept. 25.